Angewandte Chemie
Eine Zeitschrift der Gesellschaft Deutscher Chemiker

Supporting Information

Hybrid Structure of the Type 1 Pilus of Uropathogenic *Escherichia coli*

Birgit Habenstein, Antoine Loquet, Songhwan Hwang, Karin Giller, Suresh Kumar Vasa, Stefan Becker, Michael Habeck, and Adam Lange**

anie_201505065_sm_miscellaneous_information.pdf

Sample preparation

The coding sequences of full-length FimC and of FimA from amino acid 24 (without the N-terminal signal peptide) were amplified by PCR from genomic DNA of *E. coli* strain K12 (DSMZ) and cloned into the expression vector pET32a (Novagen) for producing untagged proteins. Both proteins were expressed and purified according to published protocols[1]. Uniformly ^{15}N- and ^{13}C-labeled FimA was produced in minimal medium with ^{15}N-ammonium chloride as nitrogen source and ^{13}C-glucose as carbon source. For sparse ^{13}C labelling, 2-^{13}C glycerol was used as carbon source. Pilus formation was performed as published elsewhere[2]. Typically 20 to 25 mg of FimA protein was unfolded by adding solid guanidinium hydrochloride up to a final concentration of 6 M. Subsequently the protein concentration was adjusted to 1.7 mM by ultrafiltration with a 10 kDa MWCO concentrator (Vivascience). This FimA solution was slowly added to a 20 µM FimC solution in ice-cold refolding buffer (10 mM sodium phosphate pH 7.0, 200 mM NaCl) with a final 1.2 fold (mol/mol) excess of FimC. The solution was stirred at 4 °C for 1 hour, followed by adjustment of the protein concentration to 80-90 µM. After addition of 0.02 % (w/v) sodium azide the solution was incubated for three weeks at 37 °C. Pilus formation was monitored by EM with negative staining. Finally the pili were pelleted by centrifugation at 68000 x g, washed with 10 mM sodium phosphate pH 7.0 and pelleted again. Samples were packed into 3.2 mm and 4 mm MAS rotors.

Mass-per-length measurements

STEM analyses for accurate determination of the mass-per-length (MPL) of FimA filaments were carried out at Brookhaven National Laboratory, USA. The measurements were performed on unstained freeze-dried samples at a temperature of -160 °C. The images were taken at two different dilutions (10x and 100x). For reference, tobacco mosaic virus (TMV) particles were added to the same sample and mass calibration was done by adjusting the MPL value of TMV to 13.1 kDa/Å. Image analysis was performed using the PCMass 3.2 software. In total, 18 clean images out of 64 were chosen for analysis. In each image, several chunks of FimA pili with a clear background were selected and fitted with an “8 nm solid rod” model (with a diameter of 8 nm and length of 30 nm). In total, 486 chunks were chosen and a distribution of the MPL values of these chunks was plotted.

Solid-state NMR

Solid-state NMR (ssNMR) experiments were conducted on 20 and 14.1 Tesla (^{1}H frequency of 850 MHz and 600 MHz, respectively) NMR spectrometers (Bruker Biospin, Germany), equipped with triple-resonance MAS probes (^{1}H, ^{13}C, ^{15}N) for rotor diameters of 3.2 mm and 4 mm. The sample temperature during measurements was set to 280 K (+7 °C), as measured by the water resonance relative to DSS (4,4-dimethyl-4-silapentane-1-sulphonic

acid). Chemical shifts were calibrated using DSS as internal reference[3]. Spinal-64[4] was applied for high power ^{1}H-^{13}C decoupling (amplitude of 83 kHz) during evolution and detection periods. A ramped cross-polarization with contact time of 1.2-1.75 ms was used for the initial ^{1}H-^{13}C and ^{1}H-^{15}N transfers.

[U-^{13}C, ^{15}N]-FimA sample in 4 mm rotor at 850 MHz: 2D ^{13}C-^{13}C experiments were recorded using a PDSD mixing period of 50 ms (exp. time of 1.7 days) and 175 ms (exp. time of 3.2 days) at a spinning speed of 11 kHz; and using a DARR mixing period of 50 ms (exp. time of 1.7 days) at a spinning speed of 8.33 kHz. 2D ^{15}N-^{13}C experiments (NCA and NCO) were recorded using a SPECIFIC-CP[5] transfer of 4.5 ms at a spinning speed of 11 kHz, for a total exp. time of 1 day.

[U-^{13}C, ^{15}N]-FimA sample in 3.2 mm rotor at 850 MHz: Experiments were recorded at a spinning speed of 21 kHz. A 3D ^{15}N^{13}C^{13}C (NCOCA) spectrum was recorded using a ^{15}N-^{13}C SPECIFIC-CP transfer of 5 ms and a BSH-CP[6] mixing of 4 ms (exp. time of 1 day). A 2D ^{15}N(^{13}C)^{13}C (NCACB) spectrum was recorded using a ^{15}N-^{13}C SPECIFIC-CP transfer of 5 ms and a DREAM[7] recoupling period of 2 ms (exp. time of 1 day). A 2D ^{15}N(^{13}C)^{13}C (NCACO) spectrum was recorded using a ^{15}N-^{13}C SPECIFIC-CP transfer of 5 ms and a BSH-CP mixing of 4 ms (exp. time of 2.7 days). A 3D ^{13}C^{15}N^{13}C (CANCO) spectrum was recorded using two ^{15}N-^{13}C SPECIFIC-CP transfers of 5 ms (exp. time of 3 days). A 3D ^{15}N^{13}C^{13}C (NCACO) spectrum was recorded using a ^{15}N-^{13}C SPECIFIC-CP transfer of 5 ms and a BSH-CP mixing of 4 ms (exp. time of 4.5 days). A 3D ^{15}N^{13}C^{13}C (NCACB) spectrum was recorded using a ^{15}N-^{13}C SPECIFIC-CP transfer of 5 ms and a DREAM recoupling period of 2 ms (exp. time of 3 days). A 3D ^{15}N(^{13}C)^{13}C^{13}C (NCOCACB, CO dimension not recorded) spectrum was recorded using a ^{15}N-^{13}C SPECIFIC-CP transfer of 5 ms, a ^{13}CO-^{13}CA BSH-CP mixing of 4 ms and a DREAM recoupling period of 2 ms (exp. time of 8 days).

[2-^{13}C/^{15}N]-glycerol-FimA sample in 4 mm rotor at 850 MHz: A 2D ^{13}C-^{13}C spectrum was recorded using a PDSD mixing period of 800 ms (exp. time of 13 days). The experiment was recorded at a spinning speed of 11 kHz.

[2-^{13}C/^{15}N]-glycerol-FimA sample in 4 mm rotor at 600 MHz: A 2D ^{13}C-^{13}C spectrum was recorded using a PDSD mixing period of 800 ms (exp. time of 15 days). The experiment was recorded at a spinning speed of 11 kHz.

Spectral analysis

The sequential resonance assignment was performed with a 3D assignment strategy, involving NCACB and NCACO spectra for the intra-residual correlations and CANCO,

NCOCA and N(CO)CACB spectra for the sequential connections (Figure S4). The exact peak positions were determined with the help of 2D versions of the 3D experiments using long acquisition times for achieving high resolution. Each assignment step was performed keeping at least two resonance frequencies constant as demonstrated in Figure S4. Side-chain assignment was achieved using two PDSD spectra of uniformly [^{13}C, ^{15}N] labeled pili (50 ms and 175 ms mixing times), a 3D NCACX spectrum and a 2D NCACB spectrum. A selectively [2-glycerol ^{13}C]-labeled pilus sample was used to record two PDSD spectra optimized for long-range correlation peaks to build up (mixing time of 800 ms on a 20 and a 14.1 Tesla spectrometer). The peaks from these two PDSD spectra were picked manually and assigned automatically (see *Modeling procedure*). Spectra were analyzed using the Ccpnmr Analysis software[8].

Modeling procedure

Inferential structure calculation. To calculate the structure of the FimA pilus we used the Inferential Structure Determination (ISD) software[9]. ISD applies Bayesian principles to derive a posterior probability distribution over all conformational degrees of freedom. The posterior probability distribution incorporates the experimental data as well as data-independent prior information. The prior information is based on a simple molecular mechanics force field involving a quartic repulsion term that penalizes clashes between atoms. The posterior probability distribution is used to guide a Monte Carlo procedure that generates random structures obeying the statistics of the posterior. As outlined in Habeck et al.[10] we use a combination of replica-exchange Monte Carlo and Hamiltonian Monte Carlo to sample from the complex posterior probabilities arising in biomolecular structure determination problems.

Spatial restraints from solid-state and solution NMR. 1137 distance restraints were derived from ssNMR spectra that served as a basis to determine the structure of the FimA pilus. These data were complemented with restraints derived from the solution NMR structure (2JTY) and the STEM measurements. Chemical shift and secondary structure analysis showed that FimA adopts a similar structure in the pilus assembly as in solution. Nevertheless local structural changes are to be expected, especially in the amino acids making contacts with the other subunits. These local structural differences are indicated by local discrepancies in the chemical shifts (Figure 2B and S7). Therefore we did not combine the ssNMR restraints with all of the solution NMR restraints from 2JTY. Because we expected that some of the solution and solid-state restraints would contradict each other, we

incorporated the solution NMR data only in the form of hydrogen bonds that were derived from 2JTY. The list of hydrogen bonds comprised 58 intra-molecular hydrogen bonds and was complemented by phi/psi restraints derived from the chemical shifts using the Talos+ software[11].

Representation using an exact helix symmetry. In the calculation of the structure of the FimA pilus, we only represented a single subunit explicitly using a torsion angle representation with idealized bond lengths and bond angles. All other subunits were obtained by applying the helix symmetry to the conformation of the subunit. Interactions between two subunits were projected back onto the torsion angles of the FimA protomer. In addition to the torsional degrees of freedom, we also allowed for an unknown global translation and rotation of the FimA protomer, which was sampled during the structure calculation.

Estimation of the helix symmetry with rigid-body docking. We applied rigid-body docking to estimate the helix symmetry using the self-complemented FimAa structure as rigid body where the last 19 residues forming the donor strand replaced the 19 N-terminal residues. The search space is nine-dimensional: Six parameters are the translational and rotational degrees of freedom of the rigid subunit; three additional parameters characterize the helix symmetry: radius, pitch and phase angle (the symmetry axis is known). The objective function for rigid-body docking was composed of four terms: The restraint energy from the ambiguously assigned ssNMR peaks obtained with a chemical shift tolerance of 0.2 ppm, a harmonic connectivity restraint enforcing the sequential connectivity of the subunits (the first 19 residues of the symmetry mate chemically belong to the precursor subunit), a harmonic restraint modeling the MPL obtained with STEM, and repulsive non-bonded interactions. Note that at this stage no restraints from solution NMR were used, because the solution structure itself served as subunit for rigid-body docking. During the docking procedure interactions between the FimAa subunit and 48 successive subunits obtained by applying the symmetry operator to the FimAa subunit were taken into account. The optimization was carried out with the Broyden-Fletcher-Goldfarb-Shanno (BFGS) algorithm.

MPL restraint. One problem with deriving the helix symmetry from the NMR data is that it is not possible to estimate the diameter of the helix accurately because NMR gives only local information. The missing global information was provided by a restraint on the mass-per-length (MPL). The theoretical MPL was computed by applying the helix symmetry to the center of mass of the subunit. Let L denote the distance between the initial and the final center of mass. If N subunits are taken into account, the theoretical value of the MPL is MN/L where M = 15.96 kDa is the mass of the FimA subunit. The experimental value obtained with

STEM is a MPL of 2.23±0.18 kDa/Å. To reflect the uncertainty in the experimental values we used a force constant of 1/0.174 = 33 (Å/kDa)^2.

ssNMR restraints. The ssNMR contacts were treated as ambiguous distance restraints. The upper bound was set to 7 Å for restraints derived from the 850 MHz spectrum and to 8 Å for the restraints derived from the 600 MHz spectrum. Contacts were modeled using a logistic probability model. Non-bonded interactions between six successive subunits along the pilus helix were considered. In the calculation of the ambiguous ssNMR contacts also up to six neighboring subunits were taken into account. We ran 300 independent minimizations. The lowest energy solutions formed a right-handed helix, in which the donor strand faces the barrel interior. The models based on ambiguous ssNMR restraints therefore confirm the right-handedness of the FimA pili reported by Hahn et al.[12]. The MPL of these assemblies ranges between 1.8 and 2.5 kDa/Å and is consistent with the STEM measurements; we fixed the helical rise to 7.2 Å, which is equivalent to an MPL of 2.2 kDa/Å. The pitch is 24.9 Å, the diameter of the helix is less than 75 Å. These findings are also consistent with the analysis by Hahn et al.[12].

Recalculation of the FimA protomer. Before assembling the FimA pilus, we recalculated the structure of the FimA monomer using the solution NMR restraints and starting from a completely extended conformation. Restraints involving interactions between the donor strand and the rest of the monomer were removed from the restraint list. In addition, the disulfide bridge was incorporated using harmonic distance restraints with a fixed force constant of 100 kcal/mol/Å^2. The ISD ensemble of the solution structure showed an IG fold with an RMSD of 1.01±0.14 Å to the published structure of FimAa for residues 20-159. The recalculated ensembles exhibited a higher variability than the published ensemble. Moreover, B-factors showed elevated values in the loop involving Ser90. The published structure of FimAa (2JTY) shows this loop in two conformations.

Classification of ssNMR restraints. As the next step we combined the solution restraints with the contacts from solid-state NMR. First, we used the re-calculated solution ensemble to identify ssNMR restraints that are likely to result from intra-molecular contacts. The ensemble of the FimA subunit served as a basis to classify the ssNMR restraints into intra-subunit restraints and ambiguous restraints that can be explained either as intra- or inter-subunit contacts. Restraints that were satisfied in 90% of the ensemble members, were classified as intra-subunit restraints.

Refinement of the FimA subunit using solution- and ssNMR restraints. The structure ensemble of the FimA subunit was refined using the restraints from ssNMR that were classified as intra-subunit restraints. Due to possible local conflicts between the solution and solid-state restraints, we only used hydrogen bonds derived from the previous ensemble and not the deposited solution NMR restraints. The restraints from ssNMR were modeled using a log-Laplace distribution as detailed in Shahid et al.[13].

Assembly of the FimA pilus. Using the helix symmetry obtained with rigid-body docking we computed an assembly of the FimA pilus using all restraints derived from the ssNMR spectra. The rigid-body docking calculations showed that it is sufficient to take into account the interactions between the protomer and six successive subunits obtained by applying the helix symmetry. This applies both to non-bonded interactions as well as all ambiguous ssNMR restraints that could not be classified as intra-subunit restraints previously. The ambiguous restraints are modeled as ambiguous distance restraints to which all possible distances between the protomer and its symmetry mates contribute. The three parameters of the helix symmetry were kept fixed to the values found by the rigid docking procedure. However, because we not only sampled the torsional degrees of freedom of the FimA subunit but also its global orientation and position relative to the helix axis, we can correct for errors in the rigid-body docking. The initial assembly of the protomer into the pilus structure started from the structure obtained in the recalculation of the FimA protomer. This initial ensemble of assembled FimA pilus structures with full internal flexibility served as a basis to identify intra- and inter-molecular contacts among the ambiguous restraints as described in the following paragraph.

Classification and assignment of ssNMR restraints. Based on the first ensemble of FimA structures in the pilus assembly, we tried to classify the previously ambiguous ssNMR restraints further into intra- and inter-subunit contacts. Within the inter-subunit restraints we identified contacts between subunit *i* and subunits *i-1*, *i-2*, *i-3*; any higher-order contacts were not found among the ssNMR restraints. 117 ssNMR restraints could not be classified unambiguously and were still treated as ambiguous distance restraints where contributions from all interactions with the first six subunits along the pilus helix were taken into account. We also reduced the ambiguity (due to spectral degeneracy) of the intra-subunit restraints using the following rule: Among those contributions whose chemical shifts fell within the tolerance and whose distance was smaller than a generous cutoff of 10 Å, we preferred those that were either intra-residual or sequential contacts. In case such assignments were present, all other possible assignments were discarded. If no intra-residual or sequential assignment was among all possible assignments but a contribution with a sequence

separation of two this assignment was preferred. All other ambiguous restraints were still treated as ambiguous intra-subunit restraints in the final structure calculation. This reduction in degeneracy of the intra-residual and sequential peaks doesn't bias the ensemble because it affects only the local restraints. No attempt to reduce the degeneracy of the inter-residual or fully ambiguous restraints was made. All contributions with chemical shifts matching the peak position were taken into account throughout the entire structure calculation.

Calculation of the final ensemble. Using all unambiguous and the remaining ambiguous ssNMR restraints, the final ensemble was calculated. An overview over the restraints used in this calculation and the restraint statistics is given in Table S2.

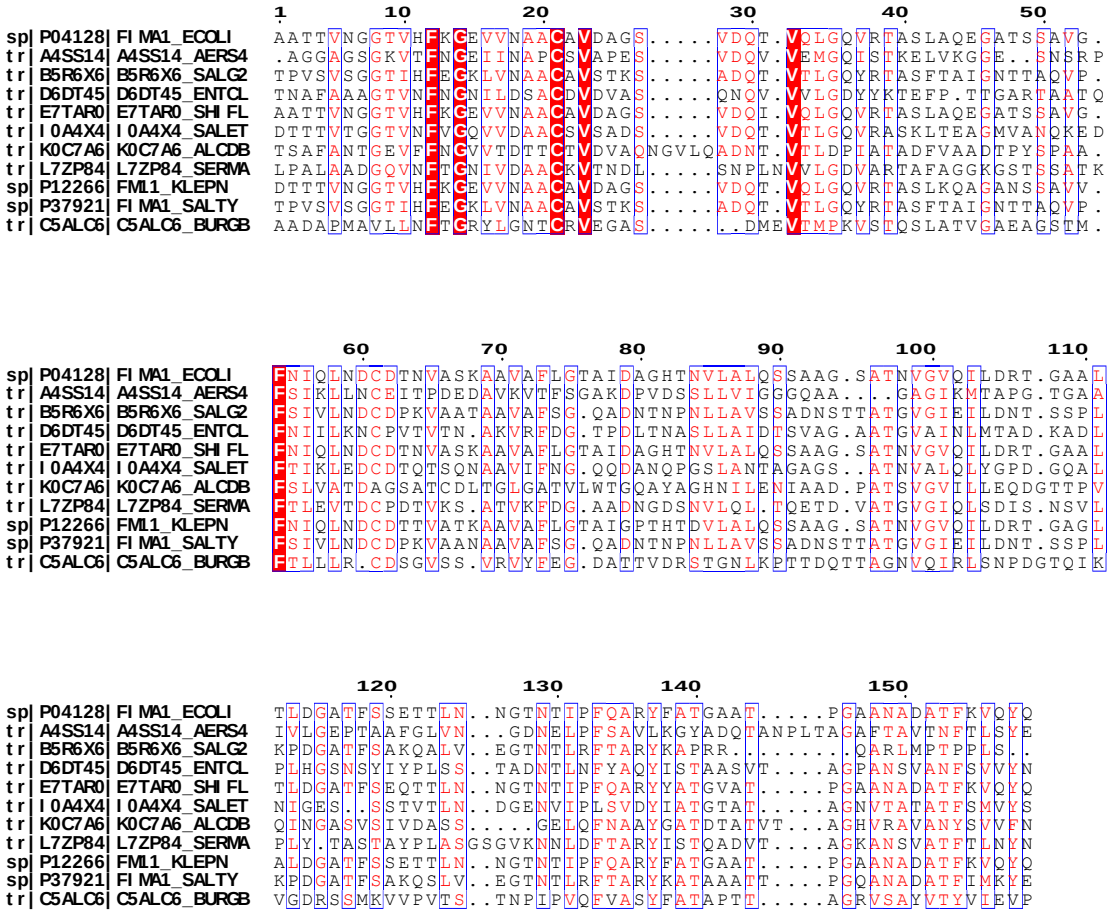

Figure S1: Sequence alignment of 11 homologous Type 1 and P pilus major pilins from different bacteria. The first line represents the here used FimA protein from uropathogenic *E. coli.* Highly conserved residues are represented on the FimA structure in Figure S11.

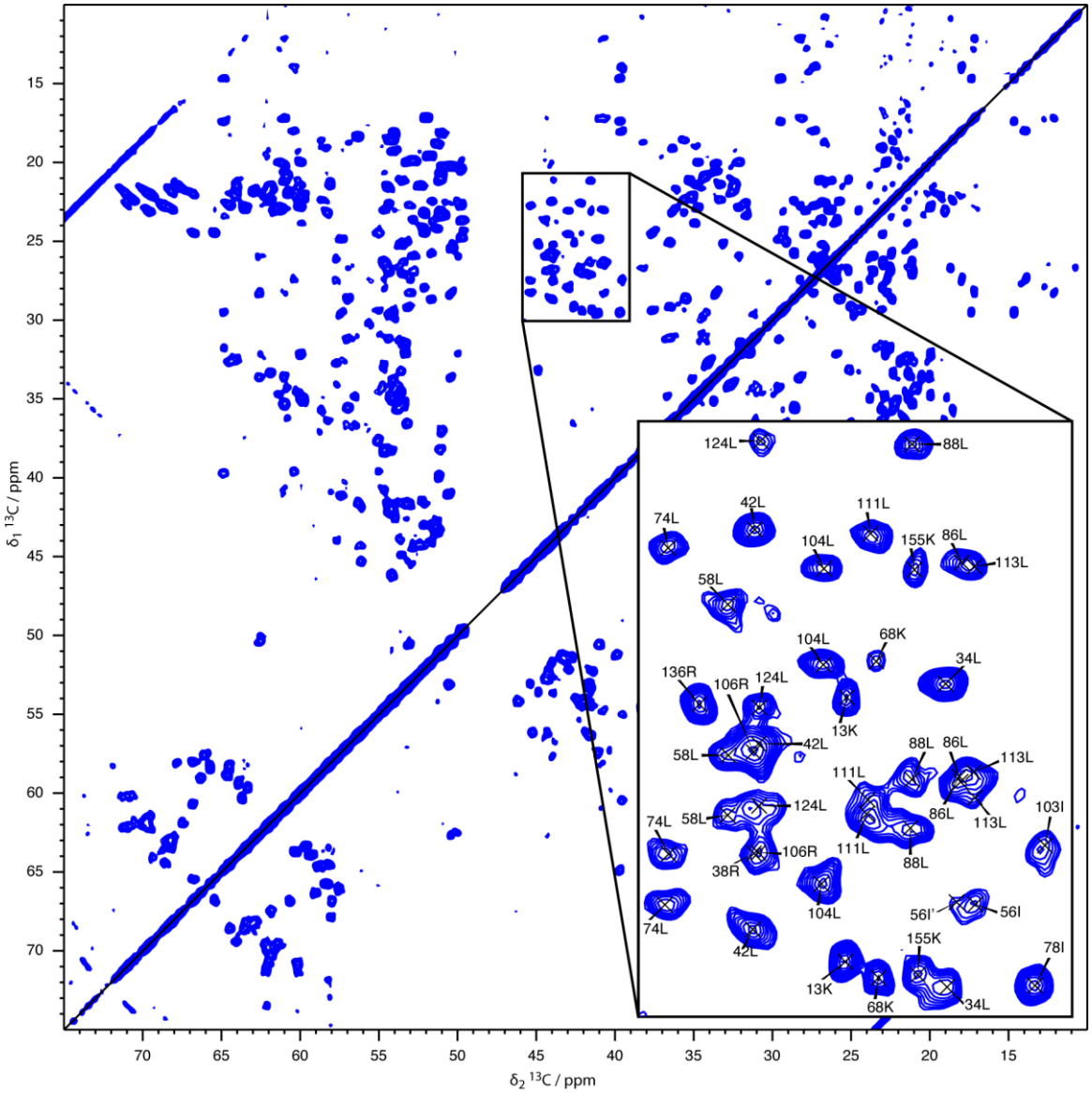

Figure S2: Solid-state NMR ^{13}C-^{13}C correlation spectrum (50 ms mixing time PDSD) of uniformly [^{13}C,^{15}N]-labeled FimA pili optimized to collect intra-residue contacts. The excerpt zooms in a selected region to illustrate the assignments.

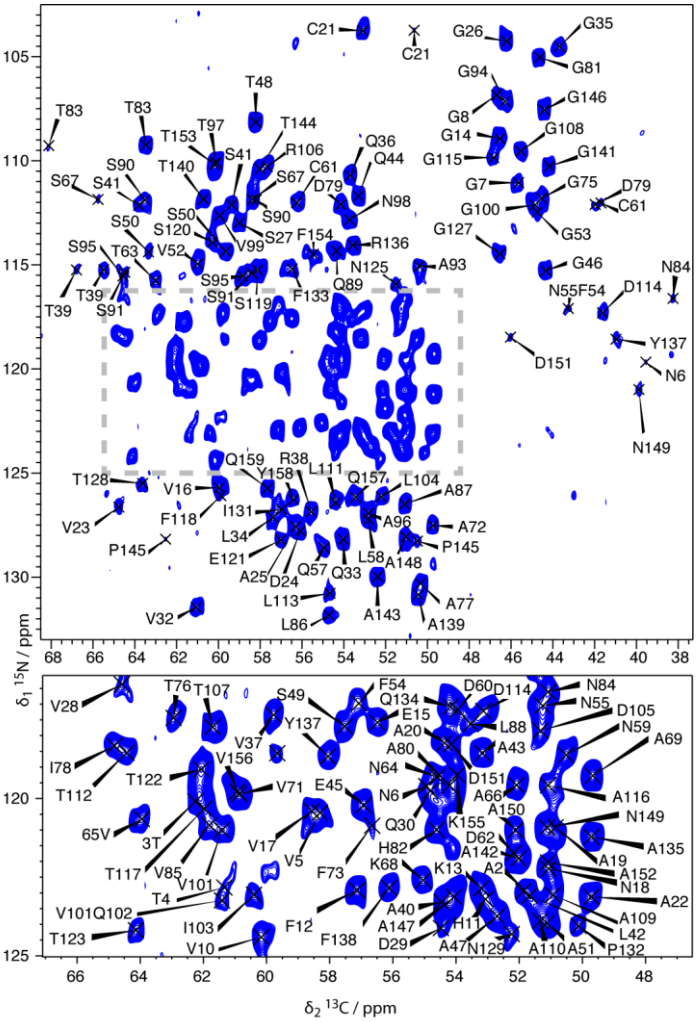

Figure S3: Solid-state NMR ^{15}N-^{13}Cα correlation spectrum of uniformly [^{13}C, ^{15}N]-labeled FimA pili. The dashed grey line indicates the spectral excerpt, as shown in the second panel.

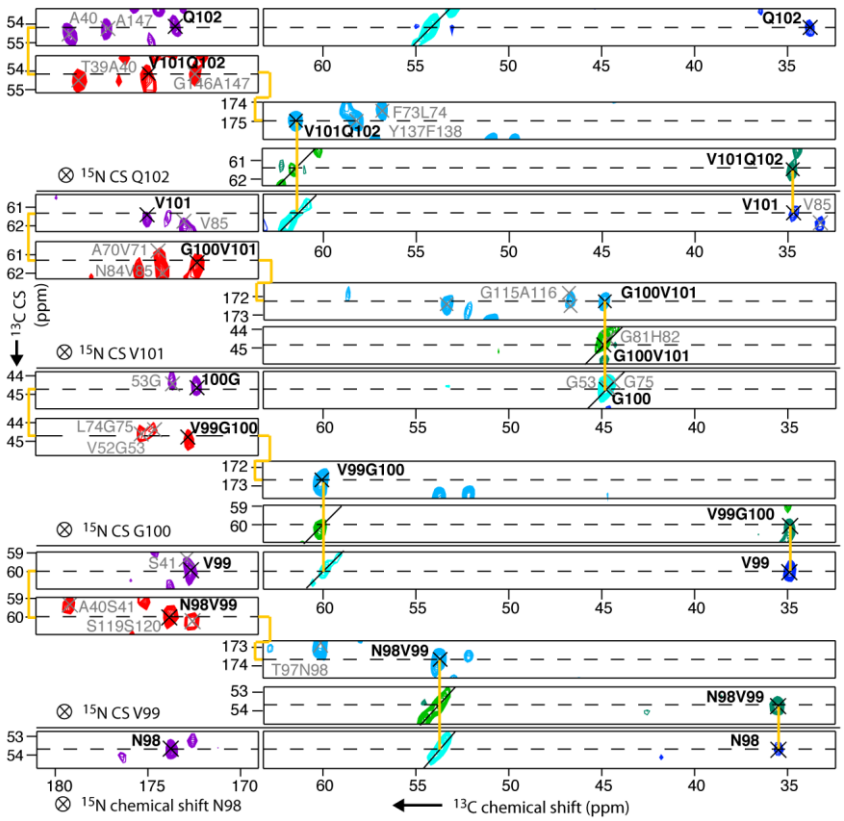

Figure S4: Sequential ssNMR resonance assignment strategy[14] used to assign FimA in pili. The determination of the ssNMR resonances was performed using a 3D sequential assignment strategy, illustrated with the stretch Q102-N98. Five strip-plots are shown, connected by yellow lines indicating constant ^{13}C resonance frequencies in each assignment step. Note the constant ^{15}N frequency of residue i. Color code of the displayed spectra (naming from above): ^{15}N-^{13}Cα-^{13}Cβ – negative value dark blue, positive light blue; ^{15}N-^{13}Cα-^{13}C' positive value purple; ^{13}Cα-^{15}N-^{13}C' – positive value red; ^{15}N-^{13}C'-^{13}Cα – positive value blue; ^{15}N-(^{13}C')-^{13}Cα-^{13}Cβ – negative value dark green, positive value light green.

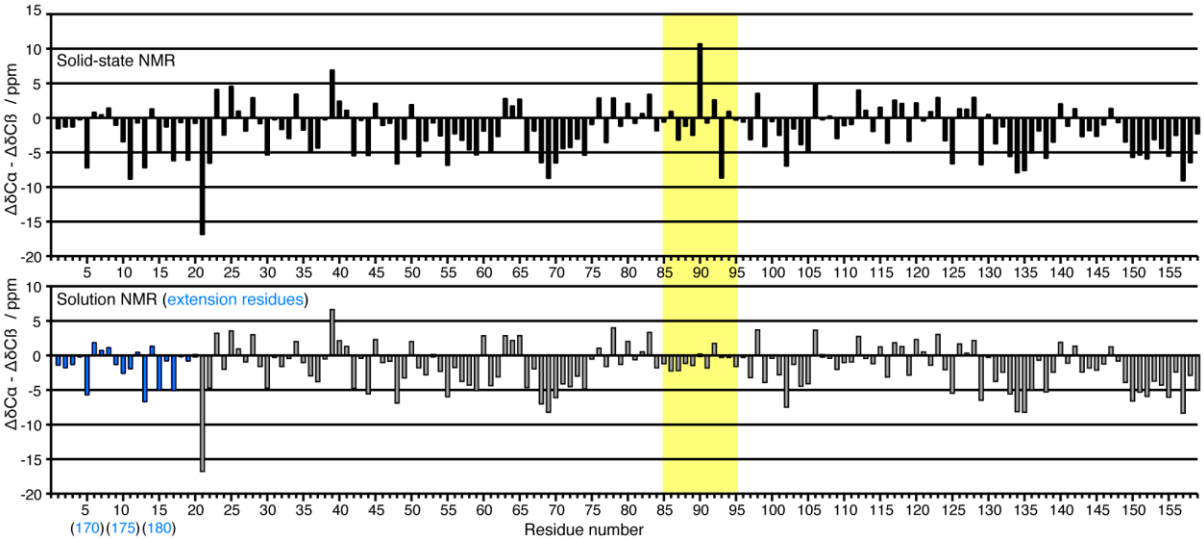

Figure S5: Secondary structure of FimA determined by the secondary chemical shift (ΔδCα-ΔδCβ) determined by solid-state NMR in the assembled pilus (black) and solution NMR in self-complemented monomers (grey). Three or more negative / positive values in a row indicate β-strand / α-helical conformation, respectively. Residues in blue indicate the artificial C-terminal extension residues of the FimAa construct that substitute the adjacent subunit's N-terminal donor strand of FimA in the pilus. Loop residues 85-95 are highlighted in yellow.

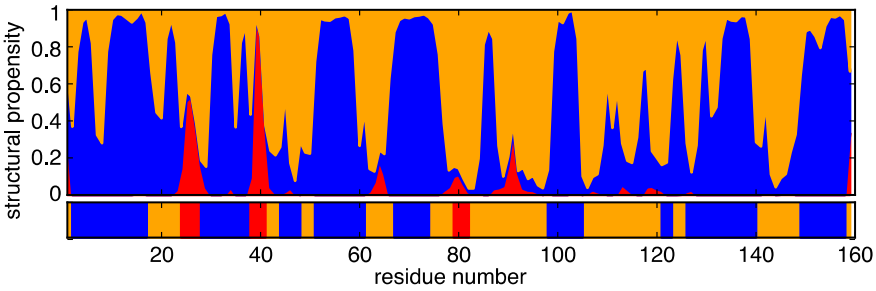

Figure S6: Secondary structure propensity of FimA in assembled pili predicted by Talos+ in the upper panel and secondary structure found in 2JTY by DSSP[15] in the lower panel (residues 1-19 are replaced by the artificial intramolecular donor strand, residues 166-184). β-strand, α-helix and coil conformational propensity are colored in blue, red and orange, respectively.

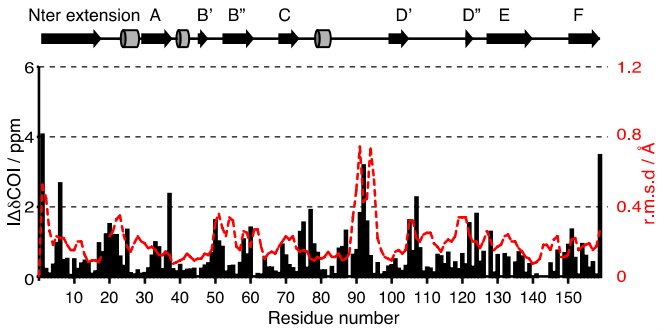

Figure S7: Secondary structure of FimA and ^{13}C chemical shift variations between the solution NMR data of artificial self-complemented FimAa monomers and solid-state NMR shifts of FimA in the assembled pili. Absolute values of Δ(solution NMR - solid-state NMR) δCO. The dashed red line indicates the backbone r.m.s.d of the solution NMR structure of the self-complemented FimAa monomer (2JTY). Residues 1-18 in 2JTY have been replaced by residues 166-183, representing the donor strand in 2JTY. The r.m.s.d. value for the connecting residue A19 has been discarded.

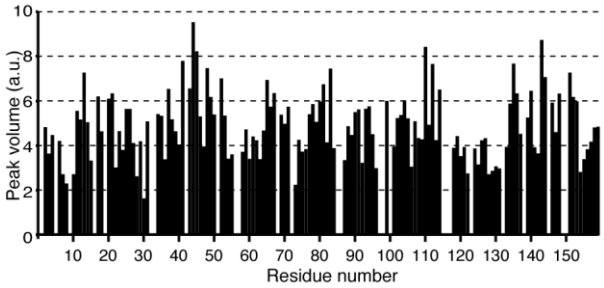

Figure S8: Peak volumes extracted from a 3D solid-state NMR NCOCA (CP / BSH-CP[6]) spectrum, recorded on a uniformly [^{13}C, ^{15}N]-labeled FimA pili sample. The volume was normalized using the noise peak volume and reflects the protein backbone rigidity. Missing volume values have been omitted due to signal overlap.

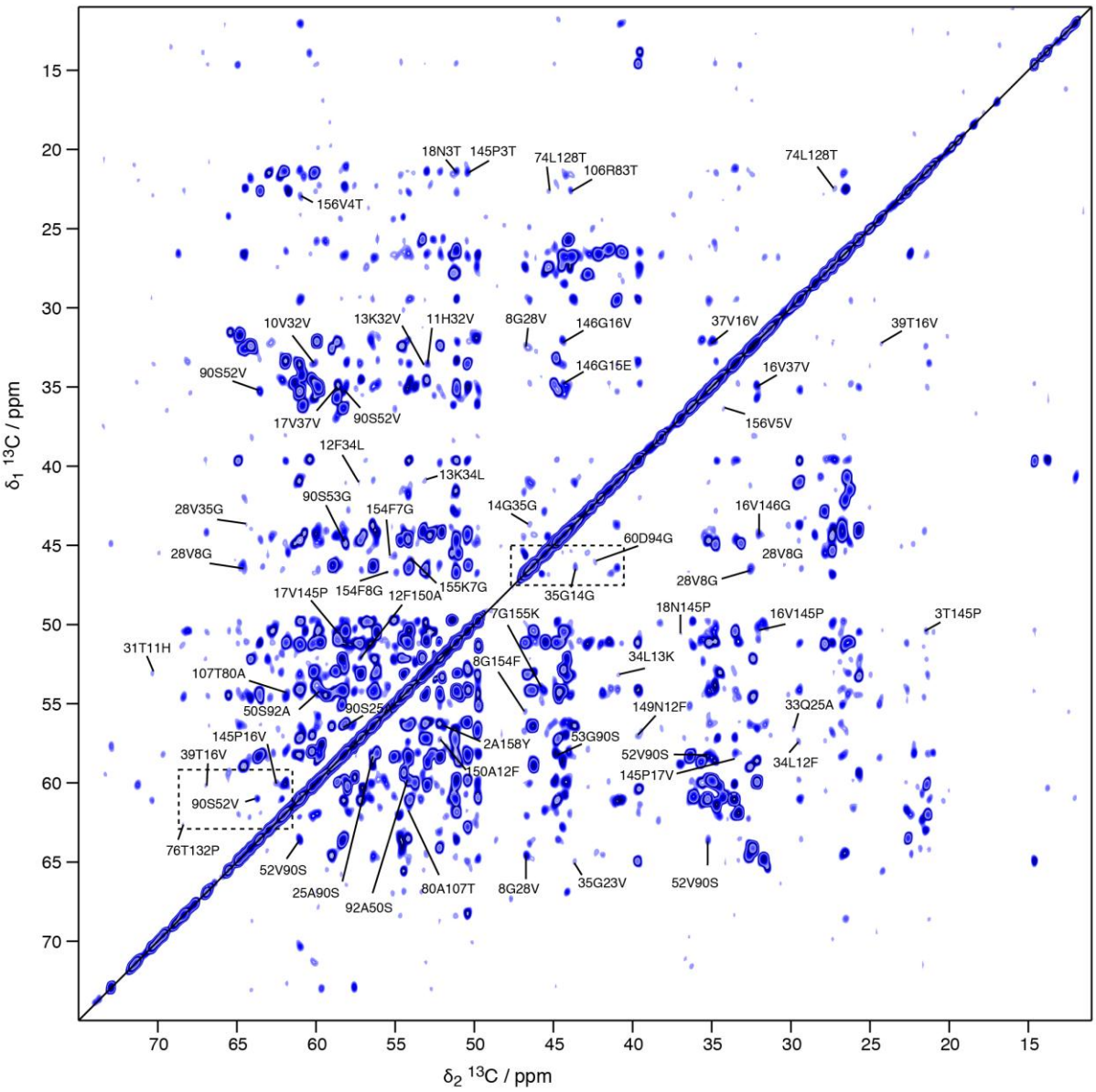

Figure S9: Solid-state NMR ^{13}C-^{13}C correlation spectrum with long mixing time (800 ms) of [2-^{13}C]-glycerol-labeled FimA pili. The spectrum was recorded on an 850 MHz spectrometer (proton resonance frequency). Inter-subunit contacts are annotated.

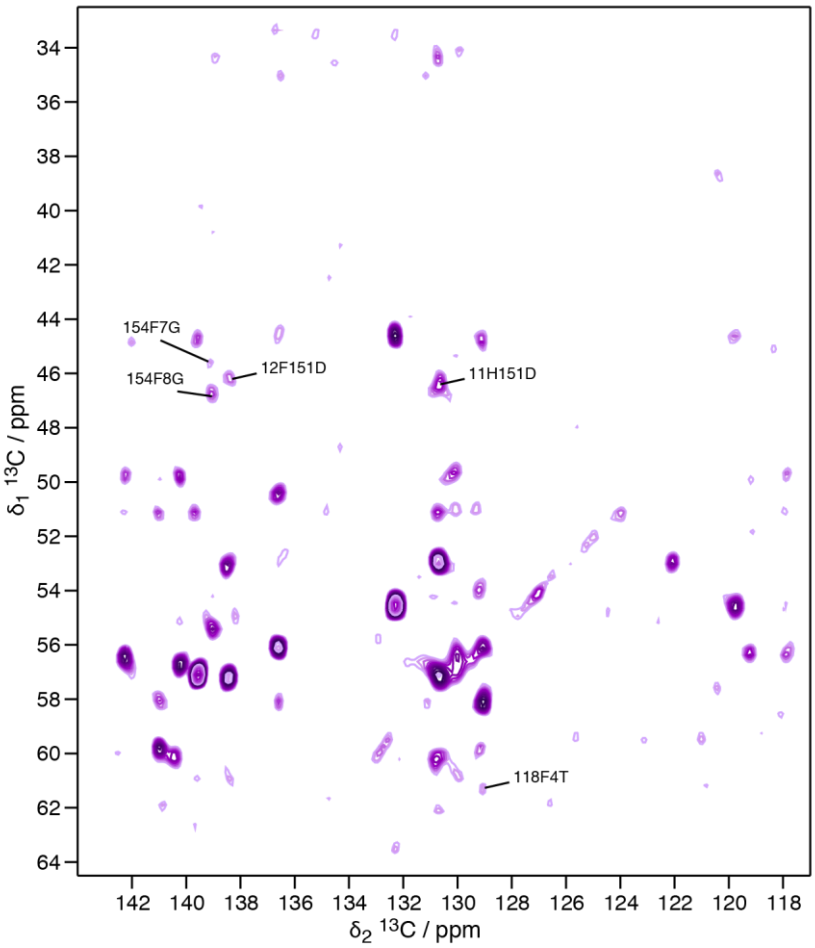

Figure S10: Solid-state NMR ^{13}C-^{13}C correlation spectrum with long mixing time (800 ms) of [2-^{13}C]-glycerol-labeled FimA pili. The spectrum was recorded on a 600 MHz spectrometer (proton resonance frequency). Excerpt of the aromatic region; inter-subunit contacts are annotated.

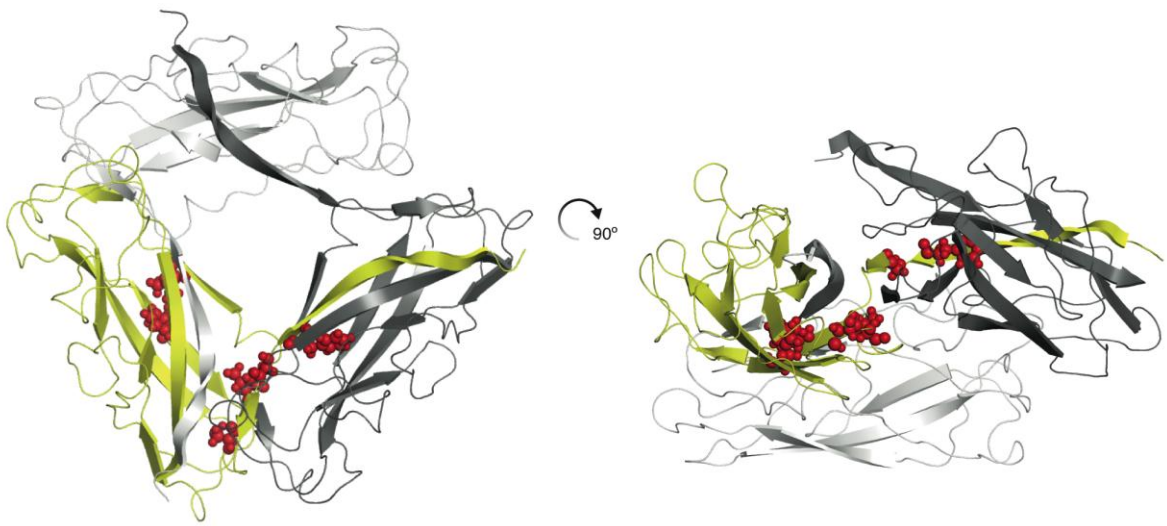

Figure S11: Highly conserved residues (see Figure S1), red sphere representation.

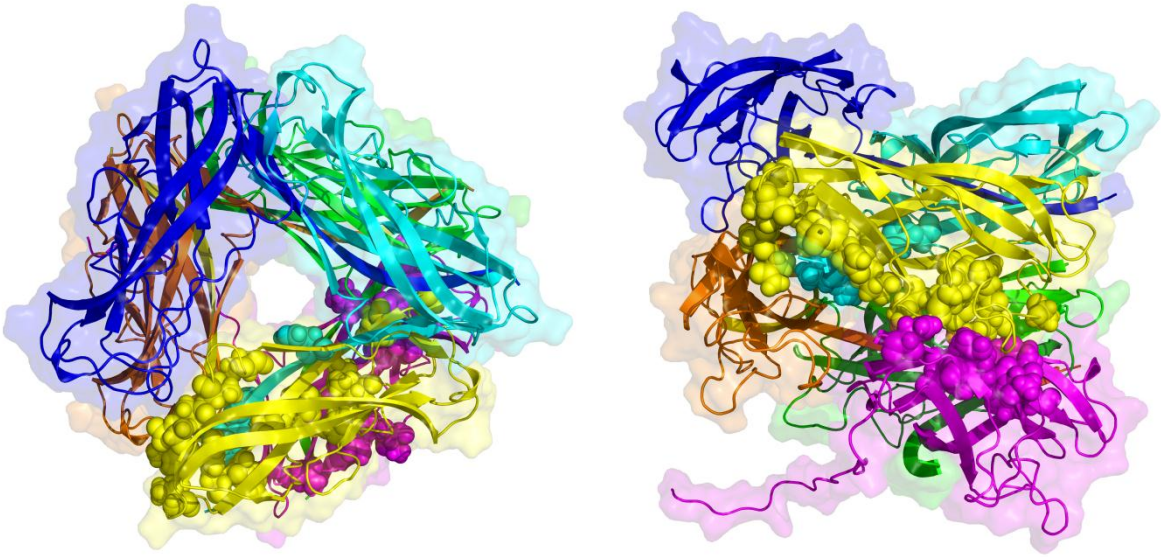

Figure S12: Top view (left) and side view (right) of the type 1 FimA pilus structure determined by solid-state NMR (PDB ID: 2MX3, present study). Space-filling models indicate the residues that exhibit absolute values of chemical shift differences larger than 1 ppm for the side chain carbons (CB, CG, CG1, CG2, CD, CD1, CD2, CE, CE1, and CZ) between solid- (present study) and solution-state NMR (BMRB ID: 15423) results. For the sake of clarity we disperse the space-filling models to three subunits (i-1, i, and i+3) and colored them as follows: Subunit i-1 (cyan): V5, N6, and H11; Subunit i (yellow): N18, A19, A22, V23, V28, D60, V65, L74, T76, L86, Q89, S90, A93, L113, K155, Q157, and Y158; Subunit i+3 (magenta): Q33, L34, Q36, A51, V52, R106, T107, T122, N125, I131, P132, A135, and Y137.

Table S1: Chemical shifts of FimA referenced internally to DSS.

Res. Number	Type	Atoms										
		N	ND	NE	NZ	C	CA	CB	CG	CD	CE	CZ
1	Ala	129.5				173.1	51.7	19.5				
2	Ala	122.9				178.0	51.9	19.5				
3	Thr	120.0				173.4	62.2	71.6	21.5			
4	Thr	122.9				174.6	61.4	69.6	22.8			
5	Val	120.4				174.4	58.3	36.3	19.1, 23.1			
6	Asn	119.6				172.3	55.0	39.5	176.7			
7	Gly	110.9				171.0	45.7					
8	Gly	106.9				172.5	46.7					
9	Thr	119.8				172.3	62.1	71.2	21.7			
10	Val	124.4				172.0	60.2	34.5	21.1, 21.6			
11	His	123.2				173.1	53.1	35.7	130.7	122.1		
12	Phe	122.9				176.2	57.2	40.4	138.5		130.6	
13	Lys	122.8				174.3	53.2	36.5	25.0	29.1	42.6	
14	Gly	108.9				173.3	46.6					
15	Glu	117.5				173.2	56.5	34.8	36.7	182.6		
16	Val	125.7				176.9	60.0	32.1	22.8, 20.0			
17	Val	120.3				174.1	58.7	35.7	22.4, 18.6			
18	Asn	122.2				173.6	51.1	37.0	177.2			
19	Ala	121.0				176.8	50.8	23.3				
20	Ala	118.1				174.5	54.4	21.5				
21	Cys	103.6				171.3	53.1	50.6				
22	Ala	123.1				175.6	49.8	22.6				
23	Val	126.6				177.1	64.9	31.7	23.4, 22.5			
24	Asp	127.8				177.2	56.1	45.2	179.6			
25	Ala	127.5				178.8	56.4	18.3				
26	Gly	104.2				175.2	46.3					
27	Ser	113.0				174.6	59.0	66.3				
28	Val	116.5				176.5	64.6	32.6	21.9, 20.1			
29	Asp	124.2				174.9	54.4	41.9	180.8			
30	Gln	119.9				173.8	54.8	32.8	34.1	181.0		
31	Thr	118.9				173.5	62.0	70.3	21.4			
32	Val	131.5				173.8	61.1	33.6	20.0, 20.6			
33	Gln	128.1				174.9	54.0	29.7	34.2	179.4		
34	Leu	127.1				177.1	57.4	41.1	29.5	23.6, 24.9		
35	Gly	104.5				172.1	43.7					
36	Gln	110.5				176.0	53.7	31.1	34.3	178.7		
37	Val	117.3				172.4	59.9	35.1	22.2, 21.9			

38	Arg	126.8		87.8		179.7	55.6	30.2	27.5	44.0		159.7
39	Thr	115.2				178.6	65.5	66.8	24.5			
40	Ala	123.3				179.2	54.5	18.5				
41	Ser	112.1				172.8	59.4	63.9				
42	Leu	123.1				174.6	51.7	44.1	25.8	28.6, 22.4		
43	Ala	118.5				176.8	53.3	19.9				
44	Gln	111.7				172.6	53.3	31.4	32.1	180.7		
45	Glu	120.2				177.5	57.0	28.6	35.5	182.6		
46	Gly	115.3				173.7	44.3					
47	Ala	123.8				175.7	52.7	19.8				
48	Thr	108.2				175.3	58.2	72.9	22.4			
49	Ser	117.7				174.6	57.5	66.0				
50	Ser	114.4				172.6	59.6	63.3				
51	Ala	124.0				176.8	51.1	23.0				
52	Val	114.9				175.3	61.0	35.2	21.1,23.0			
53	Gly	112.4				173.6	44.7					
54	Phe	117.1				171.1	57.2	42.3	139.6		130.5	
55	Asn	117.1				175.5	51.2	43.3	175.8			
56	Ile	119.7				173.7	61.0	40.9	17.2, 28.2	12.1		
57	Gln	128.6				173.6	55.0	30.9	34.4	180.3		
58	Leu	127.2				173.6	52.8	44.4	26.9	23.6, 26.0		
59	Asn	118.5				176.3	50.5	41.0	174.9			
60	Asp	117.1				174.6	53.9	42.4	180.4			
61	Cys	112.0				177.9	56.2	41.6				
62	Asp	121.8				178.1	52.3	41.5	180.0			
63	Thr	115.8				176.4	63.0	68.4	21.6			
64	Asn	119.3				176.2	54.6	38.2	177.3			
65	Val	120.8				175.6	64.0	32.4	22.7, 21.5			
66	Ala	119.6				173.5	52.1	23.2				
67	Ser	111.9				175.0	58.4	65.7				
68	Lys	122.6				174.6	55.0	37.7	24.5	29.4	42.1	
69	Ala	119.2				176.2	49.7	24.7				
70	Ala	123.5				174.4	51.3	24.2				
71	Val	119.9				174.0	60.9	36.1	22.8, 21.6			
72	Ala	127.5				176.3	49.7	20.3				
73	Phe	120.9				174.6	56.7	42.2	140.1		131.3	
74	Leu	123.5				174.5	53.0	45.4	27.4	28.3, 22.7		
75	Gly	111.8				169.6	44.5					
76	Thr	117.5				173.2	63.0	68.23	21.7			
77	Ala	130.3				177.8	50.4	20.2				
78	Ile	118.3				174.8	64.9	39.7	17.4, 29.5	14.7		

79	Asp	112.1				176.3	54.1	42.0	181.6			
80	Ala	119.5				178.4	54.2	18.5				
81	Gly	105.0				173.9	44.7					
82	His	120.9				174.6	54.6	28.0	132.3	119.8		
83	Thr	109.3				174.6	63.4	68.3	22.8			
84	Asn	116.6				174.2	51.1	38.2	177.4			
85	Val	120.9				172.9	61.9	33.3	22.4, 21.4			
86	Leu	131.7				176.0	54.7	40.8	26.3	23.0, 23.7		
87	Ala	126.4				175.7	51.1	20.6				
88	Leu	117.6				179.4	53.4	41.6	26.3	27.1, 21.1		
89	Gln	114.3				176.6	54.4	29.6	31.2	181.6		
90	Ser	111.8				173.4	63.5	58.3				
91	Ser	115.4				173.3	58.3	64.5				
92	Ala	119.7				175.2	54.1	18.0				
93	Ala	115.1				179.5	50.4	25.4				
94	Gly	107.1				174.9	46.3					
95	Ser	115.5				174.3	58.8	64.6				
96	Ala	126.8				177.2	52.9	19.8				
97	Thr	110.1				173.1	60.1	70.8,71.4	21.5			
98	Asn	112.8				173.7	53.7	35.5	178.3			
99	Val	112.6				172.7	59.9	35.0	23.8, 21.4			
100	Gly	112.1				172.3	44.9					
101	Val	121.0				174.9	61.4	34.7	22.8, 20.0			
102	Gln	123.3				173.4	54.1	33.8	35.1	179.2		
103	Ile	123.0				173.9	60.4	39.6	27.4, 18.0	13.9		
104	Leu	126.0				178.0	52.1	43.0	27.9	23.0, 24.6		
105	Asp	117.8				177.4	51.3	42.8	178.9			
106	Arg	110.3				177.7	57.7	27.5	26.0	44.0		158.9
107	Thr	117.7				173.5	61.7	67.0	22.8			
108	Gly	109.7				173.4	45.6					
109	Ala	123.0				176.2	51.0	20.2				
110	Ala	123.9				178.8	51.3	18.8				
111	Leu	126.4				177.1	54.3	42.3	26.6	26.9, 22.5		
112	Thr	118.5				174.8	64.4	68.6	22.7			
113	Leu	130.8				177.6	54.6	40.6	26.6	23.0, 26.2		
114	Asp	117.2				177.5	53.1	41.6	180.4			
115	Gly	109.9				172.0	46.8					
116	Ala	119.5				175.4	51.1	21.1				
117	Thr	120.3				173.9	61.9	67.6	21.6			
118	Phe	126.0				176.8	59.9	40.3	140.9		129.2	

119	Ser	115.2				172.5	58.0	66.8				
120	Ser	113.9				176.4	60.3	63.7				
121	Glu	128.2				177.0	57.1	31.1	36.5	182.8		
122	Thr	119.1				172.4	62.1	69.5	22.0			
123	Thr	124.2				173.6	64.1	69.4	22.1			
124	Leu	126.0				178.2	53.7	43.9	26.8	21.1, 25.2		
125	Asn	116.0				175.4	51.5	43.3				
126	Asn	121.7				178.2	54.2	38.2	176.3			
127	Gly	114.4				174.5	46.5					
128	Thr	125.6				174.4	63.7	68.9	22.7			
129	Asn	124.2				172.8	52.2	44.2				
130	Thr	120.0				172.3	62.0	69.8	21.8			
131	Ile	126.7				173.9	56.9	38.2	18.7, 26.7	10.8		
132	Pro	124.0				174.5	62.5	32.1	25.9	50.0		
133	Phe	115.1				176.1	56.5	44.5	142.2			
134	Gln	117.1				174.5	54.2	34.8	35.0	180.3		
135	Ala	121.2				175.3	49.7	23.6				
136	Arg	114.0		87.1		172.9	53.6	33.2	25.1	44.9		159.5
137	Tyr	118.6				174.9	58.1	40.9	129.1		118.0	
138	Phe	122.8				173.5	56.1	44.34	136.6			
139	Ala	130.8				175.9	50.4	20.2				
140	Thr	111.8				173.8	60.7	66.9	21.9			
141	Gly	110.2				169.5	44.2					
142	Ala	121.9				177.2	52	17.1				
143	Ala	130.1				178.1	52.42	21.4				
144	Thr	110.4				171.3	58.1	68.0	21.2			
145	Pro	128.2				176.3	62.6	33.6	28.3	50.5		
146	Gly	107.6				172.4	44.4					
147	Ala	123.1				177.2	54.1	19.2				
148	Ala	128.1				173.8	51.1	18.1				
149	Asn	120.9				173.7	51.1	39.9	176.1			
150	Ala	121.0				175.6	52.2	24.2				
151	Asp	118.3				172.8	54.2	46.1	180.7			
152	Ala	122.1				175.9	51.1	23.4				
153	Thr	110.2				173.9	60.2	71.4				
154	Phe	114.4				173.6	55.4	42.3	139.0			
155	Lys	119.2				174.2	53.9	35.6	23.1	29.4	41.5	
156	Val	119.8				173.0	61.0	34.3	21.0, 20.8			
157	Gln	126.1				173.9	53.4	35.2	34.5			
158	Tyr	126.3				175.9	56.5	43.8	130.0		117.9	
159	Gln	125.8				179.3	57.7	32.7	34.2	180.0		

Table S2: NMR constraints and refinement statistics. *NMR distances and dihedral restraints*	
Total distance constraints	1137
Intra-subunit	946
Medium range (2 < |*j*-*k*| < 5)	119
Long range (|*j*-*k*| > 4)	204
Ambiguous (due to spectral degeneracy)*	135
Inter-subunit	74
Ambiguous (intra- or inter-subunit)†	117
Hydrogen bonds	80
Intra-subunit hydrogen bonds	58
Inter-subunit hydrogen bonds (*i*) to (*i* ± *1*)	22
Total dihedral angle constraints	268
Φ	134
Ψ	134
Structure statistics	
Violated ssNMR restraints (mean ± s.d., tolerance 0.2 Å) Intramolecular / Intermolecular / Ambiguous	34.7 ± 5.0 16.9 / 1.2 / 16.6
Violated ssNMR restraints (mean ± s.d., tolerance 0.5 Å) Intramolecular / Intermolecular / Ambiguous	19.5 ± 4.8 6.5 / 0.6 / 12.4
Violated ssNMR restraints (mean ± s.d., tolerance 1.0 Å) Intramolecular / Intermolecular / Ambiguous	9.7 ± 1.6 2.6 / 0.0 / 7.1
Percentage violated ssNMR restraints (tolerance 0.2 Å) Intramolecular / Intermolecular / Ambiguous	3.1 ± 0.4 % 1.8 / 1.6 / 14.2

Percentage violated ssNMR restraints (tolerance 0.5 Å) Intramolecular / Intermolecular / Ambiguous	1.7 ± 0.4 % 0.7 / 0.8 / 10.6
Percentage violated ssNMR restraints (tolerance 1.0 Å) Intramolecular / Intermolecular / Ambiguous	0.9 ± 0.1 % 0.3 / 0.0 / 6.1
Average pairwise r.m.s.d. (Å)	
Subunit heavy atoms	1.4 ± 0.6
Subunit backbone	1.1 ± 0.4
Assembly (six subunits) heavy atoms	1.5 ± 0.6
Assembly (six subunits) backbone	1.2 ± 0.5

* Intra-subunit restraints that have more than one contributing pair of assigned atoms
† Restraints that can result from intra- or inter-subunit contacts but couldn't be classified unambiguously.

Table S3: Chemical shift differences between FimA in the solid assembled state (present study) and the soluble FimAa construct (solution NMR; BMRB ID: 15423). Blue and red colors refer to negative and positive differences. Residues highlighted in green exhibit chemical shift changes for the side chain (CB, CG, CG1, CG2, CD, CD1, CD2, CE, CE1, and CZ) of more than 1 ppm.

		C	CA	CB	CG	CG1$	CG2$	CD	CD1$	CD2$	CE	CE1	CZ
1	ALA	-4	-0.4	-0.3									
2	ALA	0.2	0	-0.5									
3	THR	0.1	0.3	0.3			0						
4	THR	0.3	-0.3	-0.4			0						
5	VAL	-0.9	-0.7	0.8		-0.4	1.3						
6	ASN	-2.6	0.3	1.3									
7	GLY	-0.5	-0.3										
8	GLY	0.5	0.3										
9	THR	0	0.1	-0.2			0.5						
10	VAL	-0.5	-0.2	0.7		-0.2	-0.6						
11	HIS	-0.2	0.1	7						0.1			
12	PHE	-0.4	-0.3	0.8								0.2	
13	LYS	-0.4	-1	-0.5	-0.5			-0.1			0.2		
14	GLY	0.4	0										
15	GLU	0.1	0.9	0.6	0.9								
16	VAL	-0.2	-0.2	0.3		-0.5	0.3						
17	VAL	-0.9	-0.4	0.7		-0.1	0.6						
18	ASN	-0.7	-2.3	-1.8									
19	ALA		-3	2.4									
20	ALA	-1.5	-0.3	0.5									
21	CYS	-1.2	0	0.1									
22	ALA	-1.2	-0.8	1									
23	VAL	0.6	1.2	0.2		0.5	1.1						
24	ASP	-0.4	0	0.5									
25	ALA	-1.4	0.6	-0.4									
26	GLY	0.1	0.1										
27	SER	0	-0.3	0.6									
28	VAL	0.2	-0.1	-0.1		0.2	-1.6						
29	ASP	-0.1	-0.1	-0.8									
30	GLN	-0.1	-0.2	0.4	0								
31	THR	-0.1	0	0			-0.2						
32	VAL	-0.6	-0.1	0		-0.2	0.4						
33	GLN	-1	-0.4	2.2	1.5								
34	LEU	-0.8	1.2	-0.2	1.6				-0.1	-0.8			
35	GLY	0.2	-0.7										
36	GLN	-0.7	-0.8	1	-0.4								
37	VAL	-2.3	-0.3	0.3		0.1	0.6						
38	ARG	0.2	-0.1	-0.5	-0.7			0.4					
39	THR	0.1	-0.2	-0.5			0.3						
40	ALA	0.3	0	-0.3									
41	SER	-0.1	0	0.2									

42	LEU	0.2	-0.4	0.3	0				-0.1	0.7			
43	ALA	0.2	0	-0.1									
44	GLN	-0.2	-0.1	-0.2	-0.2								
45	GLU	0	-0.1	0.1	0								
46	GLY	-0.2	-0.1										
47	ALA	-0.3	-0.1	-0.1									
48	THR	-0.4	-0.3	-0.6			0.4						
49	SER	0.6	0.4	0.2									
50	SER	-1.6	0	0.1									
51	ALA	-1	-0.9	2.9									
52	VAL	-0.8	-0.2	0.4		0.2	2.1						
53	GLY	-0.1	-0.7										
54	PHE	-0.2	0.3	0.7								-0.1	
55	ASN	0.3	-0.6	0.3									
56	ILE	0	0.2	0.9		0	0.2		0.3				
57	GLN	0.5	0.1	-0.4	-0.2								
58	LEU	-1.1	0.2	0.6	-0.2				0.2	0.2			
59	ASN	0.6	-0.7	-0.5									
60	ASP	-1.4	-1.3	3.3									
61	CYS		-0.6	-0.2									
62	ASP	-0.1	0	-0.5									
63	THR	-0.1	-0.1	-0.1			-0.1						
64	ASN	-0.6	-0.5	-0.1									
65	VAL	-0.3	-0.4	-0.1		0.2	1						
66	ALA	-0.3	-0.3	-0.2									
67	SER	-0.1	0.6	0.5									
68	LYS	0	0.1	-0.3	-0.3			-0.1			0		
69	ALA	0.9	-0.3	0.2									
70	ALA	-0.6	-0.1	0.4									
71	VAL	-0.2	-0.3	0		0.2	-0.4						
72	ALA	-0.2	-0.5	-0.7									
73	PHE	0.1	-0.7	-0.6								0.7	
74	LEU	-1.3	-0.6	0	-0.2				2.2	-0.7			
75	GLY	-1.5	-0.4										
76	THR	-0.3	0.4	-1.57			-0.2						
77	ALA	-1.9	-1.3	0.6									
78	ILE	0.9	-0.6	0.5		0	0.1		0				
79	ASP	0.6	0.2	0.2									
80	ALA	-0.2	0	-0.1									
81	GLY	-0.2	-0.1										
82	HIS	0	-0.1	-0.1						0.1			
83	THR	0.3	-0.2	-0.2			0.2						
84	ASN	0.1	0	0.1									
85	VAL	-0.8	0.3	-0.3		0	0						
86	LEU	-0.8	-0.3	-3.4	0.4				-3	-1.8			
87	ALA	-1.3	-0.4	0.6									
88	LEU	0	-0.1	0	0.2				0.1	-0.4			
89	GLN	-0.6	-1.4	-0.3	-2.5								
90	SER	-0.7	5.1#	-5.5#									
91	SER	-1.8	0.6	-0.4									

92	ALA	-3.2	0.1	-0.7									
93	ALA	1.5	-2.3	6.3									
94	GLY	0.5	1.1										
95	SER	-0.1	0.8	-0.5									
96	ALA	0.4	-0.3	0.1									
97	THR	0	-0.2	-0.2			-0.1						
98	ASN	0.1	-0.1	0									
99	VAL	0.3	-0.2	0.2		0.3	0.4						
100	GLY	-0.3	-0.1										
101	VAL	0.4	0.1	-0.2		0.2	0						
102	GLN	-0.2	0	-0.4	0.1								
103	ILE	-0.1	-0.4	0		0	0		0.1				
104	LEU	0.3	-0.4	-0.9	0.1				-0.3	0			
105	ASP	-1.6	-0.7	0.1									
106	ARG	0.7	-0.6	-1.8	-0.1			0.3					
107	THR	-2.3	-0.4	-3.2			0.7						
108	GLY	0.8	0.6										
109	ALA	-0.1	-0.5	0.4									
110	ALA	0.3	-0.2	0									
111	LEU	0.2	-0.2	-0.1	-0.4				0.1	-0.5			
112	THR	0.1	0.8	-0.5			-0.1						
113	LEU	0.6	-0.1	-1.5	0.1				0.2	0.4			
114	ASP	-0.6	-0.5	0.2									
115	GLY	-0.4	0.3										
116	ALA	-0.7	-0.2	0.4									
117	THR	0.2	-0.1	-0.8			0.2						
118	PHE	0.4	0.9	0									
119	SER	-0.2	-0.1	0.4									
120	SER	0.6	0.8	0.9									
121	GLU	-0.3	-0.3	0.5	0								
122	THR	-1.5	-0.4	-2.5			1.1						
123	THR	-0.3	0.6	0.7			0						
124	LEU	1.8	-0.6	0.6	0.2				-0.1	-0.1			
125	ASN	-0.4	0.4	1.5									
126	ASN	0.8	-0.3	0									
127	GLY		0.9										
128	THR	-1.3	0.2	-0.7			0.5						
129	ASN	0.1	-0.5	-0.2									
130	THR	-0.6	0.2	-0.3			-0.3						
131	ILE		-1.4	-1.4		0.2	-0.3		-2.1				
132	PRO	-0.7	0.3	-0.8	-0.4			-1					
133	PHE	0.5	-0.5	-0.5									
134	GLN	0	0	-0.2	0.6								
135	ALA	0.4	-0.8	-1.4									
136	ARG	-0.7	-0.3	-0.2				0					
137	TYR	-0.6	-0.2	1								-0.4	
138	PHE	-0.1	-0.3	0.24									
139	ALA	-0.3	-0.6	0.5									
140	THR	0	-0.1	-0.2			0.3						
141	GLY	0	-0.1										

142	ALA	0	-0.1	-0.1									
143	ALA	0	-0.08	0.2									
144	THR		-0.1	-0.1			0.1						
145	PRO	-0.4	0	0.6	0.7			0.2					
146	GLY	-0.1	0.2										
147	ALA	-0.7	-0.1	-0.2									
148	ALA	0	-0.1	-0.2									
149	ASN	-0.7	-0.2	-0.5									
150	ALA	1	0	-0.9									
151	ASP	-1.3	0.8	0.8									
152	ALA	-0.5	-0.1	0									
153	THR	0	0.1	-0.5									
154	PHE	-0.9	-0.2	0									
155	LYS	-0.6	-0.7	-1.2	-2			-0.1			-0.6		
156	VAL	-0.2	0.1	0.2		0	0.1						
157	GLN	-0.4	-0.1	0.7	-1								
158	TYR	0.1	-0.3	3.2								-0.2	
159	GLN	3.5	2.9	0.2	0.8								

$: Val CG1/CG2 and Leu CD1/CD2 were not stereospecifically assigned in the present solid-state NMR study and the chemical shift comparison thus follows the solution-state NMR assignment.

#: We note that the S90 CA/CB chemical shifts appear to be reversed between the solid- and solution-state NMR assignments.

Supporting references:

[1] a) U. Hermanns, P. Sebbel, V. Eggli, R. Glockshuber, *Biochemistry* **2000**, *39*, 11564-11570; b) C. Puorger, M. Vetsch, G. Wider, R. Glockshuber, *J. Mol. Biol.* **2011**, *412*, 520-535.

[2] M. Nishiyama, T. Ishikawa, H. Rechsteiner, R. Glockshuber, *Science* **2008**, *320*, 376-379.

[3] J. L. Markley, A. Bax, Y. Arata, C. W. Hilbers, R. Kaptein, B. D. Sykes, P. E. Wright, K. Wüthrich, *Eur. J. Biochem.* **1998**, *256*, 1-15.

[4] B. M. Fung, A. K. Khitrin, K. Ermolaev, *J. Magn. Reson.* **2000**, *142*, 97-101.

[5] M. Baldus, A. T. Petkova, J. Herzfeld, R. G. Griffin, *Mol. Phys.* **1998**, *95*, 1197-1207.

[6] V. Chevelkov, C. Shi, H. K. Fasshuber, S. Becker, A. Lange, *J. Biomol. NMR* **2013**, *56*, 303-311.

[7] R. Verel, M. Ernst, B. H. Meier, *J. Magn. Reson.* **2001**, *150*, 81-99.

[8] a) W. F. Vranken, W. Boucher, T. J. Stevens, R. H. Fogh, A. Pajon, M. Llinas, E. L. Ulrich, J. L. Markley, J. Ionides, E. D. Laue, *Proteins* **2005**, *59*, 687-696; b) T. J. Stevens, R. H. Fogh, W. Boucher, V. A. Higman, F. Eisenmenger, B. Bardiaux, B. J. van Rossum, H. Oschkinat, E. D. Laue, *J. Biomol. NMR* **2011**, *51*, 437-447.

[9] a) W. Rieping, M. Habeck, M. Nilges, *Science* **2005**, *309*, 303-306; b) W. Rieping, M. Nilges, M. Habeck, *Bioinformatics* **2008**, *24*, 1104-1105.

[10] M. Habeck, M. Nilges, W. Rieping, *Phys. Rev. Lett.* **2005**, *94*, 018105.

[11] Y. Shen, F. Delaglio, G. Cornilescu, A. Bax, *J. Biomol. NMR* **2009**, *44*, 213-223.

[12] E. Hahn, P. Wild, U. Hermanns, P. Sebbel, R. Glockshuber, M. Haner, N. Taschner, P. Burkhard, U. Aebi, S. A. Muller, *J. Mol. Biol.* **2002**, *323*, 845-857.

[13] S. A. Shahid, B. Bardiaux, W. T. Franks, L. Krabben, M. Habeck, B. J. van Rossum, D. Linke, *Nat. Methods* **2012**, *9*, 1212-1217.

[14] C. Shi, H. K. Fasshuber, V. Chevelkov, S. Xiang, B. Habenstein, S. K. Vasa, S. Becker, A. Lange, *J. Biomol. NMR* **2014**, *59*, 15-22.
[15] a) W. Kabsch, C. Sander, *Biopolymers* **1983**, *22*, 2577-2637; b) R. P. Joosten, T. A. te Beek, E. Krieger, M. L. Hekkelman, R. W. Hooft, R. Schneider, C. Sander, G. Vriend, *Nucleic Acids Res.* **2011**, *39*, D411-419.